Dependence of neutron yield on the deuterium filling pressure in a plasma focus device

2004 Plasma Phys. Control. Fusion 46 1095

(http://iopscience.iop.org/0741-3335/46/7/009)

INSTITUTE OF PHYSICS PUBLISHING PLASMA PHYSICS AND CONTROLLED FUSION

Plasma Phys. Control. Fusion **46** (2004) 1095–1104 PII: S0741-3335(04)74030-0

Dependence of neutron yield on the deuterium filling pressure in a plasma focus device

Hyun-Jong Woo, Kyu-Sun Chung and Myoung-Jae Lee

electric Probe Applications Laboratory (ePAL), Hanyang University, 17 Haengdang, Seongdong, Seoul 133-791, Korea

E-mail: kschung@hanyang.ac.kr

Received 18 December 2003
Published 4 June 2004
Online at stacks.iop.org/PPCF/46/1095
doi:10.1088/0741-3335/46/7/009

Abstract

A Mather-type plasma focus device (32 μF, 4 kJ), called Hanyang University Plasma Focus device, is developed as a prototype device for the irradiation test of neutrons for electric probes and cables to be used in Korea Superconducting Tokamak Advanced Research with pure deuterium gas. The six different lengths of electrode are used in order to see the dependence of neutron yield on the deuterium filling pressure at given system conditions such as capacitance, currents and inductance, after optimizing the focusing condition in terms of electrode length versus filling pressure. The relationship between the pressure and electrode length is to be fitted well by the snow-plow model. The neutron fluence and angular distribution are measured at the angles of 0°, 25°, 60° and 90° by locating the bubble neutron dosimeter at a distance 30 cm from the inner electrode head at each electrode length. The anisotropic factor tends to increase with pressure and the total neutron yield is strongly dependent on the isotropic emission. The maximum neutron yield is estimated to be about 1.6×10^8 (n/shot) at a pressure of 3.4 Torr.

1. Introduction

The plasma focus device (PFD) is based on the z-pinch phenomenon, which is caused by the self-generating azimuthal magnetic induction due to high current in the axial direction. The PFD can be classified as Filippov-type (Filippov *et al* 1962) and Mather-type (Mather 1964, Mather and Bottoms 1968) according to the aspect ratio of the inner electrode length (z_0) to its diameter (D), i.e. $z_0/D < 1$ and $z_0/D > 1$ for Filippov-type and Mather-type, respectively. This classification is also to be made according to the cathode geometry (open or closed), or position of insulator with respect to anode. Generally, the PFD produces radiation such as x-rays, electrons, ions and neutrons with deuterium gas due to very fast compression and heating of plasmas related to self-generating high magnetic induction. Since the work of

Filippov and Mather, the PFD has been developed as a radiation generator more extensively during the last three decades, and it is known as the most powerful laboratory neutron source, so that it can be used as a neutron irradiation device for the test of the electric probes and fusion materials used at fusion devices such as Korea Superconducting Tokamak Advanced Research (KSTAR) and International Thermonuclear Experimental Reactor (ITER).

Although the details of the mechanism of neutron generation from the PFD are not clear, the following three mechanisms are plausible: first, the neutrons are generated as the result of the thermonuclear fusion reaction in the neck formed during the development of the $m = 0$ instability (Vikhrev 1986, Moreno *et al* 2000), yet this model could not explain the anisotropic neutron emission sufficiently. Second, the beam–target model indicates that the neutrons are generated due to the acceleration of non-thermal ions in the neck by the induction of strong electric fields (Bernstein 1970, Bernstein and Comisar 1972, Tiseanu *et al* 1994, Zhukov *et al* 2001). Last, the converging ion model maintains that the neutrons are generated when the ions impinge into a small space centred at the region of collapse (Lee *et al* 1971).

Despite the absence of a convincing mechanism of neutron generation, experiments have clarified the mechanism and improved the performance of the PFD. The materials of electrodes and insulator are related to the generation of the impurity of plasma and current sheet, which was studied by Zakaullah *et al* (1993), Rout *et al* (1995) and Shyam and Rout (1997). The common result of these efforts is that the highest neutron yield is achieved using a combination of tungsten electrode and quartz insulator because this gives less impurity to plasma and current sheet. The correlation between non-uniform density of deuterium gas and neutron yield was studied at the PACO device by Milanese *et al* (1998). According to this, the anisotropic emission is increased when the gas cloud is moved parallel to axis, that is, the probability of beam–target processes is enhanced. Nevertheless, this is not enough to improve the total neutron yield. Kelly and Márquez (1996) suggested through the experiments on the PF-II device, that the ions with low energy are important in neutron production and that the actual neutron yield is dependent on the beam–target collisions between fast ions and background gases. Springham *et al* (2000) also suggested that ion beam density and neutron yield are closely correlated. Castillo *et al* (2000, 2003) maintained that the thermonuclear fusion and beam–target mechanisms co-exist from the evidence of soft x-ray emission due to bremsstrahlung and hard x-ray emission due to interactions between high energy electron and electrode surface, respectively. Antanasijević *et al* (1999) and Castillo *et al* (2003) have shown that the neutron angular distribution has a Gaussian function when pure deuterium gas is used as the filling gas. They also observed that the neutron angular distribution has a tendency to become isotropic with argon–deuterium mixture. Dependence of neutron yield on the deuterium filling pressure was studied by Zakaullah *et al* (1995, 1998, 1999) and they explained indirectly that neutrons are generated by two mechanisms, namely thermonuclear fusion and beam–target reactions.

To measure the neutron production, a bubble neutron dosimeter is widely used in various areas for its advantages (Smirnova *et al* 1992, Ing 1997, 2001): (i) insensitivity to gamma-radiation, (ii) dependence of linear neutron yield upon energy up to 20 MeV, (iii) high response efficiency, (iv) small size compared to other neutron detectors and (v) easy calculation of neutron yield by digitized picture of bubbles without using a sophisticated data acquisition system.

We developed the PFD, called Hanyang University Plasma Focus (HUPF) device, as a prototype device for the irradiation test of neutrons for electric probes and cables to be used in KSTAR. This work is focused on the dependence of neutron yield on the filling pressure under plasma conditions such as magnetic induction and implosion time. For this, six different electrode lengths are used in order to find the optimized focusing condition since the filling pressure is strongly correlated with electrode length at the same discharge parameters such

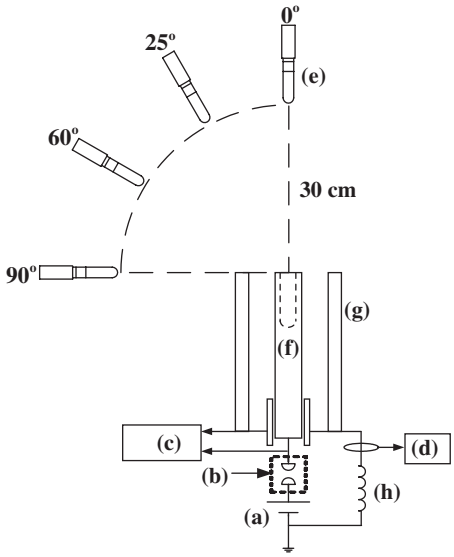

Figure 1. Schematic diagram of the HUPF device: (*a*) 32 μF (maximum 40 kV) capacitor, (*b*) triggered spark gap switch, (*c*) 1000 : 1 high voltage probe, (*d*) Pearson coil, (*e*) BD-PND, (*f*) inner electrode, (*g*) outer electrode and (*h*) stray inductance.

as capacitance, inductance, resistance, inductance and electrode geometry. This procedure is necessary to understand the neutron generation mechanism and to optimize a HUPF device as a neutron source. The experimental set-up is described in section 2, and section 3 covers the experimental results and analysis. Finally, section 4 summarizes our work.

2. Experimental set-up

The HUPF device is energized by a 32 μF (25 kJ) single capacitor charged up to 16 kV (4 kJ). The arrangement of electrodes and diagnostic systems is schematically shown in figure 1. The oxygen-free copper inner electrode, with a diameter of 20 mm, has a hollow shape at the end to reduce interaction between the electron beam generated from the HUPF device and the electrode surface at the focus region. The outer electrode is composed of sixteen copper rods with diameter of 10 mm, which forms the shape of a squirrel cage with an inner diameter of 70 mm. The 1.5 mm thick quartz tube, with a breakdown length of 13 mm, is located between the inner and the outer electrode as an insulator. Six different electrode lengths (14.5, 16, 17, 18, 20.5 and 22 cm) are used in order to see the neutron yield dependence on the deuterium filling pressure under the same conditions of magnetic induction, and the last five data in fifteen shots in each electrode are taken. Since one needs conditioning for each new electrode, we take ten shots for conditioning and check the consistent repeatability of current and voltage drops at each electrode length. A rotary pump is used to provide the base vacuum up to 20 mTorr and the triggered field distortion spark gap switch connects the inner electrode to the positively charged terminal of the capacitor bank.

The discharge voltage is measured with a high voltage resistive probe between the inner and outer electrodes and the current is measured with Pearson coil model No 101. As the maximum current allowed is 50 kA for the Pearson coil, the ground line of the HUPF device is divided into seven sub-lines and the discharge current is measured from one of the seven lines

with the Pearson coil. The typical discharge current has a rise time (one quarter time period) of 3.85 μs and a peak current of 183 kA.

For the time-integrated neutron measurement, bubble detector-personal neutron dosimeter (BD-PND) from Bubble Technology Institute (BTI) is used. The BD-PND is based on the phase transition of superheated-liquid–vapour. It consists of microscopic droplets of ^{6}Li dispersed through the elastic polymer. When a neutron strikes these droplets, α-particles are generated from ^{6}Li (n, α) T reaction and the energy from these α-particles triggers the microscopic droplets to explode immediately. The resulting gas bubbles, which are visible, are trapped in the elastic polymer medium and the number of bubbles is directly proportional to the neutron equivalent dose (Ing 1997, Vanhavere *et al* 1998). Ing (2001) studied the dependence of the response of the BD-PND on the irradiated neutron angles. Smirnova *et al* (1992) verified the efficiency of the bubble neutron dosimeter for fusion neutron detection from Tokamak-10, Tokamak-15 and the PFD. It is located at a distance of 30 cm and at angles of 0°, 25°, 60° and 90° from the inner electrode head (or axis). Before the neutron measurement from the HUPF device, the bubble dosimeter is calibrated with ^{241}Am–Be (4.3 MeV) neutron sources on its side face in the Korea Atomic Energy Research Institute (KAERI). From this calibration, we noticed that the signal from our bubble dosimeter is 20% higher than that indicated in the original manual, and we take this account into our measurement. In this experiment, the neutrons are irradiated to the bottom part of the bubble dosimeters which are distributed at different angles to measure the neutron angular distribution with higher resolution. According to the work of Ing (2001), the conversion factor from neutron dose equivalent to fluence is 3×10^{-5} (mrem/neutrons) and the response is 0.35, which is the ratio of measured neutrons through the side part to the bottom part. That is, the conversion factor is about 9.524×10^4 n cm^{-2} mrem^{-1}. The main components of the bubble counting systems are a CCD camera, a diffusion screen, a lamp and a beaker filled with water. The CCD camera is interfaced to a computer running a commercial image processing program (Image-Pro Plus: Media Cybermetics, Inc.). The bubble dosimeter is placed in the beaker filled with water. After turning on the lamp, some adjustments are made to focus the CCD camera in order to classify the bubble irradiated by neutrons from the small droplets. Then, the number of bubbles is calculated by using an image processing program.

3. Experimental results and data analysis

The characteristic axial transit time, by which the current sheet approaches the top of the inner electrode for the focusing, is explained using the snow-plow model,

$$t_p = \left[\frac{4\pi^2\left(c^2-1\right)}{\mu \ln c}\right]^{1/2} \frac{z_0 \rho_0^{1/2}}{(I_0/a)}, \tag{1}$$

where t_p, a, b, μ, z_0, I_0 and ρ_0 are axial transit time, radius of inner electrode, radius of outer electrode, permeability, length of inner electrode, characteristic current and ambient gas density, respectively and $c = b/a$ (Lee and Serban 1996). The focus system would be optimized if the input current passing through the electrode is maximum. This occurs when the focusing is generated, i.e. when the current sheet (plasma) formed between the electrodes reaches the top of the inner electrode and is focused. Then it maximizes the magnetic induction and leads to optimium plasma focus. In other words, the plasma axial transit time is equal to the quarter time period, and then it becomes the optimized condition for the PFD (Moreno *et al* 2000). We obtained the optimum pressure with a certain electrode, i.e. when the voltage peak and current drop occur at the quarter time period, by changing the filling pressure for optimum

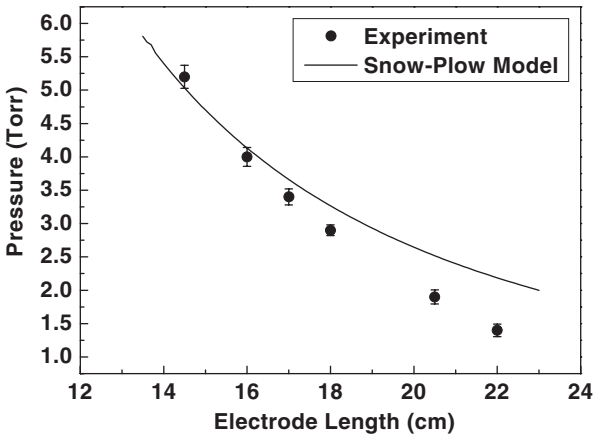

Figure 2. Optimum deuterium filling pressure related to the electrode lengths.

focusing condition, and then duplicated this process for the six electrodes with different lengths as shown in figure 2. Figure 2 shows the relationship between optimum filling pressure and electrode length at one quarter time period. The experimental data seem to follow the snow-plow model, equation (1), although there is a slight difference as electrode length is increased. It might be conjectured that the deviation from the prediction of the snow-plow model is due to the decrease of the plasma current, $\boldsymbol{J}_{\mathrm{p}}$ (or the force of $\boldsymbol{J}_{\mathrm{p}}\times\boldsymbol{B}_{\theta}$). This conjecture is based on the increasing probability of recombination process with more impurities that are added to the current sheet (or plasma) as it travels a longer distance from the bottom to the top of the electrodes. When the plasma is focused, the voltage spike and current drop are observed as the impedance of the plasma increases due to $m = 0$ instability and these are shown in figure 3. From these, it has been found that the characteristic current is about 183 kA and the characteristic axial transit time is about 3.85 μs.

Figure 4 represents the angular distributions of neutrons with different electrode lengths and pressures under the assumption that the neutrons are generated azimuthally symmetric because of the co-axial geometry of the electrode. The angular distributions of neutrons measured from the HUPF device are adjusted by a Gaussian function, related to the anisotropic emission. Although the data are insufficient at the angle from 0° to 25°, they agree well with the results of PACO device (Castillo *et al* 2003). Figure 5 shows the dependence of neutron fluence on the filling pressure. The neutron fluence at an angle of 0° has a tendency to increase rapidly with increasing pressure up to 3 Torr and saturates over the pressure of 3 Torr. However, the neutron fluence measured from the other angles is rarely changed. This implies that the anisotropic factor increases with the pressure. This is shown more clearly in figure 6, where the ratio of neutron fluence at an angle of 0° to that at other angles is plotted. The subscript α indicates the angles of 25°, 60° and 90°. The anisotropic factor has a general tendency to increase with the deuterium filling pressure.

To calculate the total neutron yields, the Gaussian function is used as shown in figure 4, and is given by

$$f(\theta) = A + \frac{B}{w\sqrt{\pi/2}} \exp\left[-2\frac{\theta^2}{w^2}\right], \tag{2}$$

where A is a constant, B is the area, w is the width in radians and θ is the angle in radians. The total neutron yield (Y_{T}) can be calculated from surface integration of equation (2) with

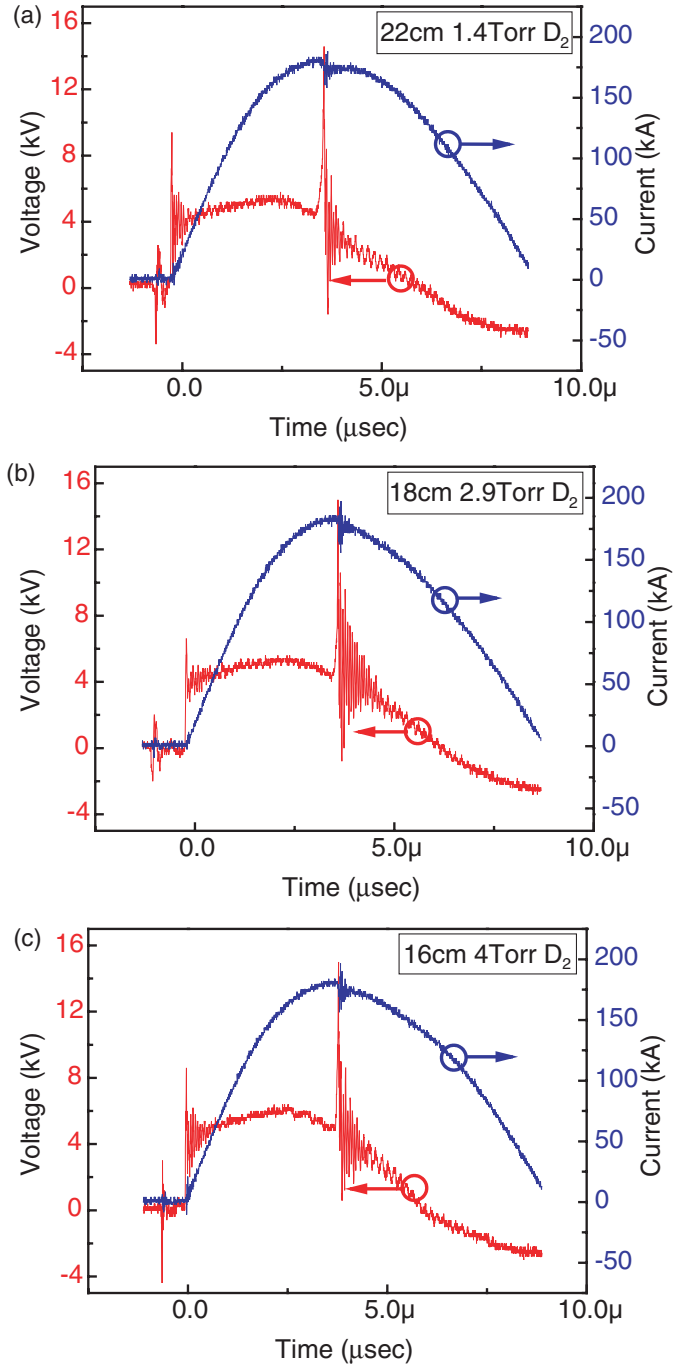

Figure 3. Voltages and current signal for optimized condition: (*a*) 22 cm–1.4 Torr, (*b*) 18 cm–2.9 Torr and (*c*) 16 cm–4.0 Torr.

(This figure is in colour only in the electronic version)

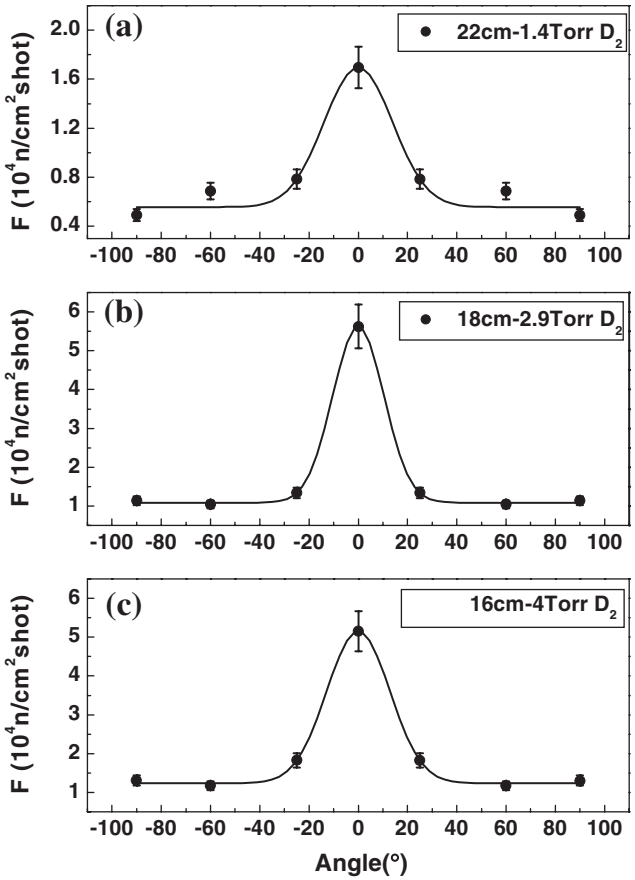

Figure 4. Neutron angular distributions, F = neutron fluence: (*a*) optimum pressure: 1.4 Torr and length of electrode = 22 cm, (*b*) optimum pressure: 2.9 Torr and length of electrode = 18 cm and (*c*) optimum pressure: 4.0 Torr and length of electrode = 16 cm.

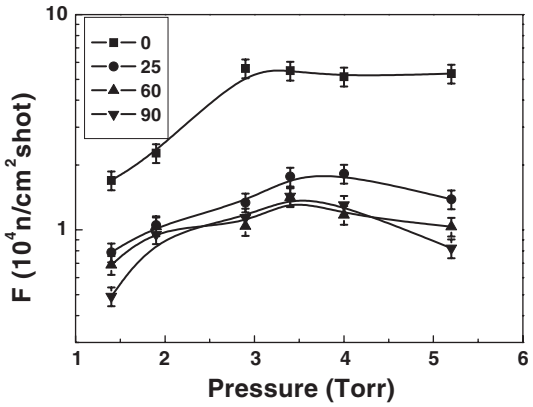

Figure 5. Dependence of neutron fluence on the filling pressure, F = neutron fluence: solid square is for the angle of 0°, solid circle is for the angle of 25°, solid triangle is for the angle of 60° and solid inverse triangle is for the angle of 90°.

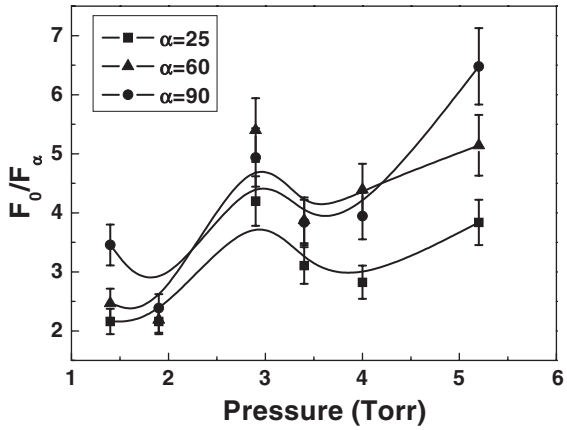

Figure 6. Dependence of anisotropic factors on the filling pressure: solid square is for the angle of 25°, solid triangle is for the angle of 60° and solid circle is for the angle of 90°.

Table 1. Components of Gaussian distribution and neutron yield: A, B and w represent the constant, area and width in equation (3) and Y_{I}, Y_{A} and Y_{T} are the isotropic, anisotropic and total contributions of neutron yield, respectively.

Optimum pressure (Torr)	Electrode length (cm)	$A \times 10^4$	$B \times 10^3$	w (radian) $\times 10^{-2}$	$Y_{\mathrm{I}} \times 10^8$	$Y_{\mathrm{A}} \times 10^5$	$Y_{\mathrm{T}} \times 10^8$
1.4	22	0.589	1.040	7.469	0.666	0.873	0.667
1.9	20.5	0.996	0.888	5.551	1.126	0.556	1.127
2.9	18	1.091	3.278	5.766	1.233	2.131	1.235
3.4	17	1.425	3.181	6.244	1.611	2.240	1.613
4	16	1.239	3.492	7.123	1.402	2.804	1.405
5.2	14.5	0.928	3.596	6.534	1.049	2.649	1.052

spherical geometry:

$$Y_{\mathrm{T}} = 4\pi r^2 A + 2\pi r^2 \int_0^{\pi} \frac{B}{w\sqrt{\pi/2}} \exp\left[-2\frac{\theta^2}{w^2}\right] \mathrm{d}\theta, \tag{3}$$

where r is the distance of BD-PND from the anode head. In equation (3), the first term is the isotropic contribution, Y_{I}, and the latter is the anisotropic one, Y_{A}. The corresponding results for each case are given in table 1 and also shown in figure 7. The isotropic and anisotropic contributions of neutron yields are all dependent on the pressure. However, the tendencies of the two contributions are different. The anisotropic contribution increases steadily with the pressure and then saturates. On the other hand, the isotropic contribution increases up to 3.5 Torr, and then decreases. The neutron yield has a parabola-like function with the deuterium filling pressure and the maximum neutron yields are estimated to be about 1.6×10^8 (n/shot) at a pressure of 3.4 Torr with electrode length of 17 cm. The anisotropic contribution, Y_{A}, is estimated about 2.8×10^5 (n/shot) at a pressure of 4 Torr with electrode length of 16 cm.

4. Conclusions

The dependence of neutron yield on the deuterium filling pressure is measured using the HUPF device by means of the bubble neutron dosimeter, after optimizing the focusing condition by controlling the length of the electrodes. The optimum pressure seems to fit well

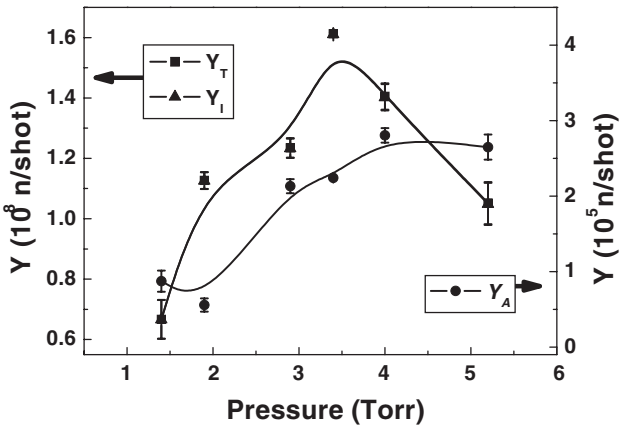

Figure 7. Dependence of neutron yield on the filling pressure, Y = neutron yield: solid squares, triangles and circles represent the neutron yield of total, isotropic and anisotropic contributions, respectively.

with the snow-plow model. Although there are not enough experimental data points for the angles of 0–25° in figure 4, it may be assumed that the neutrons are generated spatially with Gaussian distributions based upon the earlier work (Antanasijević *et al* 1999, Castillo *et al* 2003). In addition, the isotropic and anisotropic contributions have different tendencies of variation with the filling pressure. Although the anisotropic factor has a small value in the 3.5 Torr pressure region, it has a general tendency to increase with pressure. This is a result different from that of Zakaullah *et al* (1995) with respect to the magnitude of the anisotropic factor and its tendency. The total neutron yield depends strongly on the isotropic contribution and has the shape of a parabola-like function with the deuterium filling pressure. It agrees well with the model of Moreno *et al* (2000) and the experimental results of Zakaullah *et al* (1995, 1998, 1999). The neutron yield and optimized condition are deduced as 1.6×10^8 (n/shot) and 3.4 Torr at an electrode length of 17 cm.

The different tendencies of the isotropic and anisotropic contributions seem to be related to the variation of the thermonuclear fusion cross-section and the interaction probability between the deuteron beam and the background gas. From these results, the neutrons are expected to be generated by the combined reactions of thermonuclear fusion and beam–target reaction, i.e. the isotropic contribution would be based on the thermonuclear fusion and anisotropic emission based on the beam–target reaction. It would be better for the understanding of the detailed mechanism of neutron generation if the ion energy, ion angular distribution, neutron energy and time-resolved neutron fluence were to be measured with the operating pressures.

Acknowledgments

This work was supported by the National Research Laboratory (NRL) project of the Korea Institute of Science and Technology Evaluation and Planning (KISTEP) under the Ministry of Science and Technology (MOST) of Korea. The authors would like to express thanks to Hyun-Jong You, Yong-Sup Choi and Dr Yong Ho Jung of ePAL for the technical support, to Professor Jai-Ki Lee of Hanyang University for the bubble dosimetry and its calibration, and to Professors Eiki Hotta and Kazuhiko Horioka of the Tokyo Institute of Technology for their keen comments. Constructive and insightful comments of the referees are greatly appreciated.

References

Antanasijević R, Marić Z, Banjanac R, Dragić A, Stanojević J, Åoråević D, Joksimović D, Udovičić V and Voković J 1999 *Radiat. Meas.* **31** 443

Bernstein M J 1970 *Phys. Rev. Lett.* **24** 724

Bernstein M J and Comisar G G 1972 *Phys. Fluids* **15** 700

Castillo F, Milanese M, Moroso R and Pouzo J 2000 *J. Phys. D: Appl. Phys.* **34** 141

Castillo F, Herrera J J E, Rangel J, Milanese M, Moroso R, Pouzo J, Golzarri J I and Espinosa G 2003 *Plasma Phys. Control. Fusion* **45** 289

Filippov N V, Filippova T I and Vinogradov V P 1962 *Nucl. Fusion Suppl.* **2** 577

Ing H 1997 *Radiat. Meas.* **27** 1

Ing H 2001 *Radiat. Meas.* **33** 275

Kelly H and Márquez A 1996 *Plasma Phys. Control. Fusion* **38** 1931

Lee J H, Shomo L P, Willams M D and Hermansdorfer H 1971 *Phys. Fluids* **14** 2217

Lee S and Serban A 1996 *IEEE Trans. Plasma Sci.* **24** 1101

Mather J W 1964 *Phys. Fluids Suppl.* **7** 28

Mather J W and Bottoms P J 1968 *Phys. Fluids* **11** 611

Milanese M, Moroso R and Pouzo J 1998 *J. Phys. D: Appl. Phys.* **31** 85

Moreno C, Bruzzone H, Martinez J and Clausse A 2000 *IEEE Trans. Plasma Sci.* **28** 1735

Rout R K, Garg A B, Shyam A and Srinivasan M 1995 *IEEE Trans. Plasma Sci.* **23** 996

Shyam A and Rout R K 1997 *IEEE Trans. Plasma Sci.* **25** 1166

Smirnova N, Semaschko N and Martinuk Y 1992 *Radiat. Prot. Dosimetry* **44** 347

Springham S V, Lee S and Rafique M S 2000 *Plasma Phys. Control. Fusion* **42** 1023

Tiseanu I, Mandache N and Zambreanu V 1994 *Plasma Phys. Control. Fusion* **36** 417

Vanhavere F, Loos M, Plompen A J, Wattecamps E and Thierens H 1998 *Radiat. Meas.* **29** 573

Vikhrev V V 1986 *Sov. J. Plasma Phys.* **12** 262

Zakaullah M, Ahmed I, Rashid N, Murtaza G and Beg M M 1993 *Plasma Phys. Control. Fusion* **35** 689

Zakaullah M, Akhtar I, Murtaza G and Waheed A 1999 *Phys. Plasmas* **6** 3188

Zakaullah M, Akhtar I, Waheed A, Alamgir K, Shah A Z and Murtaza G 1998 *Plasma Sources Sci. Technol.* **7** 206

Zakaullah M, Murtaza G, Ahmad I, Beg F N, Beg M M and Shabbir M 1995 *Plasma Sources Sci. Technol.* **4** 117

Zhukov Yu N, Markoliya A I, Popov A I and Chachakov A F 2001 *Techn. Phys.* **46** 1379